MRS Advances © 2016 Materials Research Society
DOI: 10.1557/adv.2016.628

Effect of Li, Fe, and B Addition on the Crystallization Behavior of Sodium Aluminosilicate Glasses as Analogues for Hanford High Level Waste Glasses

José Marcial[1], Mostafa Ahmadzadeh[1], John S. McCloy[1,2]

[1] Materials Science and Engineering Program, Washington State University, Pullman, WA 99164, USA

[2] School of Mechanical and Materials Engineering, Washington State University, Pullman, WA 99164, USA

ABSTRACT

Crystallization of aluminosilicates during the conversion of Hanford high-level waste (HLW) to glass is a function of the composition of the glass-forming melt. In high-sodium, high-aluminum waste streams, the crystallization of nepheline ($NaAlSiO_4$) removes chemically durable glass-formers from the melt, leaving behind a residual melt that is enriched in less durable components, such as sodium and boron. We seek to further understand the effect of lithium, boron, and iron addition on the crystallization of model silicate glasses as analogues for the complex waste glass. Boron and iron behave as glass intermediates which allow for crystallization when present in low additions but frustrate crystallization in high additions. In this work, we seek to compare the average structures of quenched and heat treated glasses through Raman spectroscopy, X-ray diffraction, vibrating sample magnetometry, and X-ray pair distribution function analysis. The endmembers of this study are feldspathoid-like ($LiAlSiO_4$, $NaAlSiO_4$, $NaBSiO_4$, and $NaFeSiO_4$), pyroxene-like ($LiAlSi_2O_6$, $NaAlSi_2O_6$, $NaBSi_2O_6$, and $NaFeSi_2O_6$), and feldspar-like ($LiAlSi_3O_8$, $NaAlSi_3O_8$, $NaBSi_3O_8$, and $NaFeSi_3O_8$). Such a comparison will provide further insight on the complex relationship between the average chemical ordering and topology of glass on crystallization.

INTRODUCTION

The Hanford site in southeastern Washington state currently stores 177 underground tanks that house over 200,000 m^3 of nuclear waste that was generated from the 1940's through the late 1980's [1]. This waste will be separated into two categories: low activity waste and high level waste. Low activity waste will constitute approximately 90 mass percent while high level waste (HLW) will constitute over 95 percent of the radioactivity [1]. Waste will be mixed with glass-forming additives (e.g., SiO_2 and H_3BO_3) and vitrified in a large-scale melter at the Waste Treatment and Immobilization Plant (WTP) currently under construction. The resulting melt from feed decomposition will be poured into canisters and transferred to a permanent repository.

Currently formulations of Hanford HLW glass are particularly high in Na_2O, Al_2O_3, and SiO_2. Compositional restrictions must be placed to prevent the crystallization upon cooling along the centerline of the canister, since the crystallization reduces the chemical durability of the final waste form. The crystallization behavior of silicate melts can be markedly influenced by (i) the makeup of the network forming and intermediate compounds (e.g., Al_2O_3, B_2O_3, Fe_2O_3, and SiO_2) and (ii) the makeup of the network modifying compounds (e.g., Li_2O, and Na_2O).

These effects of the composition are believed to manifest in the kinetics of crystallization and whether crystal nucleation is homogeneous or heterogeneous.

Typical phases observed to crystallize from HLW glasses during lab-scale experiments include spinel and aluminosilicates [1]. The crystallization of aluminosilicate phases results in the chemical partitioning of chemically durable constituents such as SiO_2 and Al_2O_3 into the crystalline phase. Due to chemical partitioning, there exists a residual amorphous phase enriched in constituents with significantly lower chemical durability, e.g. alkali and boron oxides [2, 3]. The prototypical aluminosilicate phase observed to crystallize from Hanford HLW glasses is nepheline, mineralogically $Na_{0.75}K_{0.25}AlSiO_4$ [1-3]. However, with the large compositional space of Hanford HLW, various components are believed to substitute into the nepheline, including Li_2O and Fe_2O_3 [4-6]. Additional silicate and aluminosilicate phases have been observed to form in HLW glasses and are adversely impact the chemical durability (e.g., β-eucryptite, $LiAlSiO_4$, and aegirine, $NaFeSi_2O_6$) [2, 3, 5, 7]. Crystallization of spinel and transition metal oxides also occurs, but has not been found to negatively affect chemical durability [2, 3]. Similar to Hanford HLW glasses, HLW glasses generated in the United Kingdom may form spinel and silicate phase upon cooling [8].

Phases such as nepheline and β-eucryptite, along with their polymorphs, are feldspathoids, rock-forming minerals comprised of a framework of $[SiO_{4/2}]$ and $[AlO_{4/2}]$ tetrahedral units mostly arranged in a network of hexagonal and distorted six-membered rings [9, 10]. These phases are known as stuffed derivatives of various silica polymorphs. "Stuffed derivative" signifies that these phases feature large similarities to a particular silica framework (for example, tridymite) but differ because half of the Si atoms have been replaced with Al atoms, and a charge-compensating cation has been "stuffed" into the channels of the framework in order to provide charge compensation for $[AlO_{4/2}]$ units [9, 10]. Nominally the endmembers of feldspathoid minerals are represented with a Si/Al ratio equal to unity, whereas pyroxene and feldspar mineral endmembers feature Si/Al=2 and 3, respectively. In the case of B and Fe substituted glasses, the assumption is that these ions substitute in in the tetrahedral (*T*) position for Al, with some potential differences due to valence and coordination changes.

In this study, the choice of the network modifying atoms was restricted to either Na or Li. The choice of the network forming atom was restricted to Si, and three intermediates were used (Al, B, or Fe). We will seek to compare the crystallization behavior of feldspathoid, pyroxene, and feldspar glasses as analogues for HLW glasses. Within glasses, iron occurs in two valence states (2+ and 3+) where the different oxygen coordinations for iron are four- five- and six-fold, while boron is 3+ and three-or four-fold coordinated by oxygen [6].

EXPERIMENTAL DETAILS

Glasses were prepared by mixing powders of Li_2CO_3, Na_2CO_3, Al_2O_3, H_3BO_3, Fe_2O_3, and SiO_2 following a standard melt-quenching method. The mixed powders were melted at temperatures ranging from 1050°C to 1650°C, depending upon the composition, in Pt-10% Rh crucibles in air. Crystallization was performed either isothermally or slow cooled as follows: 1500-850°C at 10 K min^{-1} then furnace cooled from 850-330°C as in [11]. The endmember compositions prepared were $LiAlSiO_4$, $NaAlSiO_4$, $NaBSiO_4$, and $NaFeSiO_4$ (feldspathoid-like); $LiAlSi_2O_6$, $NaAlSi_2O_6$, $NaBSi_2O_6$, and $NaFeSi_2O_6$, (pyroxene-like); $LiAlSi_3O_8$, $NaAlSi_3O_8$, $NaBSi_3O_8$, and $NaFeSi_3O_8$ (feldspar-like).

XRD scans were performed using a PANalytical X'Pert Pro diffractometer with Cu-K_α X-ray source at 45 keV and 40 mA and a X'Celerator© 1-D solid state detector as in [11]. X-ray pair distribution functions (XPDFs) were measured using the same diffractometer with a Ag-K_α X-ray source at 60 keV and 36 mA and a scintillator detector with a variable counting time (VCT) scans in the range from 2-120° 2θ with a 0.06° 2θ step. For Rietveld analysis, samples were doped with 5 or 10 wt% CaF_2 internal standard and analyzed using Highscore software (PANalytical, The Netherlands). VCT data was transformed to XPDFs, G(r), using PDFgetX2© software using Q_{max}=14 Å, compositional corrections, and 1/E quadratic Compton scattering correction [12].

Raman spectroscopy was performed using a Renishaw InVia Raman microscope (United Kingdom) outfitted with a Leica optical microscope. Raman spectra were collected from 1600-250 cm^{-1} using the 442 nm line of a He-Cd laser at full laser power and an exposure time of 10 s as in [11]. Fluorescence background was stripped with Fityk software (Warsaw, Poland) [13].

Magnetic measurements of the iron-containing samples were performed with a PMC3900 Vibrating sample magnetometer (VSM) (Lakeshore Cryotronics, Westerville, OH) with maximum applied field of 18 kOe at room temperature.

RESULTS

Upon slow cooling of the feldspathoid-like glass, $NaAlSiO_4$ glass crystallized 5 wt% cubic carnegieite and 87.4 wt% orthorhombic carnegieite, and $LiAlSiO_4$ glass crystallized 75.2 wt% β-eucryptite whose crystallographic information files (CIF) can be found in literature [14-16]. The $NaFeSiO_4$ glass crystallized magnetite (Fe_3O_4) upon quenching, and hematite (Fe_2O_3) after heat-treating at 900°C for 24 hrs (CIFs can be found in the references [17, 18]). Of the pyroxene-like glasses, $NaFeSi_2O_6$ glass was found to crystallize and formed aegirine, $NaFe^{(III)}Si_2O_6$, upon isothermal cooling at 900°C for 24 hrs. None of the feldspar-like glasses were found to crystallize.

Figure 1 provides the XPDFs and Raman spectra for the glasses and crystalline species. Figure 2 depicts the network structure of tridymite projected down the [001] plane and highlights some common O-O distances drawn using VESTA 3 software [19, 20]. Figure 3 provides the magnetic hysteresis loops for the heat-treated Fe-bearing glasses.

DISCUSSION

Comparison of the XPDFs of the as-quenched aluminosilicate glasses with the crystalline samples reveals similarities among the patterns of the Li-bearing glasses (LAS) and β-eucryptite in the range of 1-5.5 Å, as well as the patterns of the Na-bearing glasses (NAS) with nepheline mineral and albite mineral in the range of 1-4.5 Å. Taylor and Brown [21] previously found Mo Kα XPDFs of NAS glasses (those with stoichiometry for Si/Al = 1, 2, and 3) more closely resemble that of mineral nepheline than the other sodium aluminosilicate minerals. Here, small features increase as a function of Si/Al ratio at 3 and 5 Å in the patterns of all glasses. Deconvolution of calculated XPDFs for crystalline feldspathoid phases reveal that the correlations located near 3 and 5 Å are attributed to O-O where the 2.5-3 Å coordinations are on the order for adjacent apical O atoms in polyhedral units. Correlations on the order of 4-4.5 Å are for O atoms across 4-member rings such as those in albite ($NaAlSi_3O_8$) and correlations of 5-5.5 Å are on the order for O atoms across symmetric 6-member rings such as those in tridymite

(SiO_2), see Figure 2. Tridymite does not crystallize from melt and therefore an increase in these units may elucidate why the addition of SiO_2 hinders crystallization in HLW glasses [6].

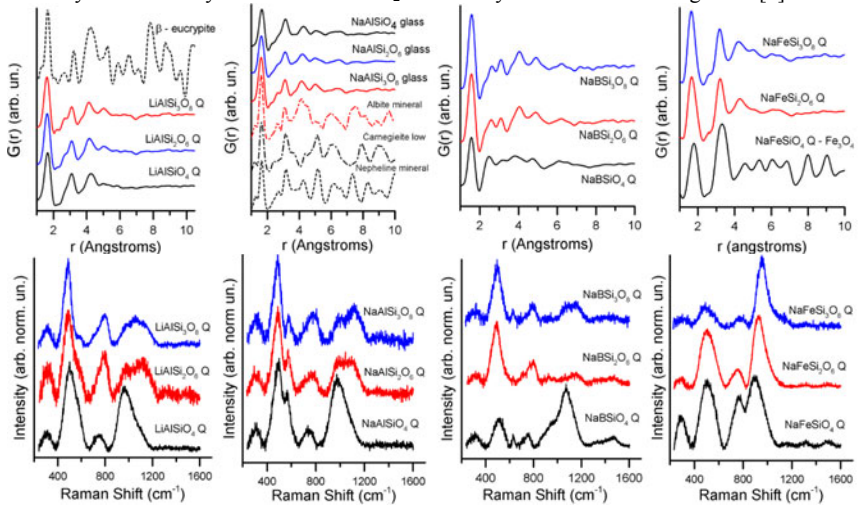

Figure 1. XPDFs (top) and Raman spectra (bottom) of glasses (Q) and crystalline phases of LAS, NAS, NBS, and NFS (left to right). The feldspathoid-like systems are shown in black, the pyroxene-like in red, and the feldspar-like in blue (color online).

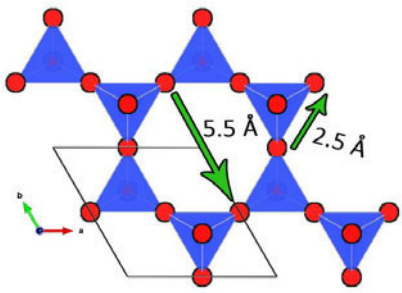

Figure 2. Depiction of the network structure of tridymite showing some common O-O distances

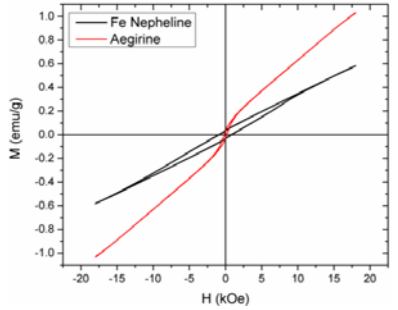

Figure 3. Magnetic hysteresis loops showing magnetization (M) as a function of applied field (H) for the heat-treated Fe-bearing glasses

Raman spectra of the as-quenched NAS, LAS, and NBS glasses tend to feature an increase in the Raman band in the range of 600-800 cm^{-1} and a decrease or splitting of the band in the range of 800-1200 cm^{-1} as a function of Si addition. The NFS glasses feature a decreasing trend in the 600-800 cm^{-1} band but also a left shift in the 800-1200 cm^{-1} with increased silica addition. Raman bands in the range of 850-1200 cm^{-1} have been assigned to the antisymmetric stretching modes of *T*-O which is generally attributed to the motion of a tetrahedral cation within its oxygen

cage [22, 23]. We assume that most of the *T* species exist as tetrahedra which are bonded to four-tetrahedral neighbors (Q^4) and therefore the differences among the Raman spectra are the consequence of multiple ring structures in the as-quenched glasses where a broader peak width has been attributed to a broad distribution in the ring sizes [22, 23]. The Raman spectra for the NBS glasses feature a 630 and 1460 cm^{-1} bands in agreement with the work of Pierce et al [24] who attributed these bands to ring meta borate and ring B_2O_3 moieties.

Heat treatment trials of Fe-nepheline ($NaFeSiO_4$) found that this endmember will not crystallize in agreement with the work of Onuma et al [25] where it was hypothesized that this phase is metastable and will spontaneously decompose to aegirine ($NaFeSi_2O_6$), 5-1-8 ($Na_5FeSi_4O_{12}$), and hematite (Fe_2O_3). Hematite was the only crystalline phase that formed upon heat-treating Fe-nepheline. The so-called Fe-albite ($NaFeSi_3O_8$) endmember also does not crystallize from melt. Aegirine, on the other hand, formed upon isothermally heat-treating $NaFeSi_2O_6$ glasses at 900°C for 24 hr.

The magnetic properties of the samples discussed here are the result of the ordering of the Fe atoms. Previous authors [26, 27] have reported that aegirine is an antiferromagnetic phase with a very low Néel temperature, suggesting that it is paramagnetic at room temperature. In the present study, the magnetic hysteresis loop of synthesized aegirine (Figure 2) shows a relatively high magnetization and a ferrimagnetic behavior. The observed magnetic properties of aegirine can be due to the presence of a small fraction of possible magnetite ($Fe^{(II)}Fe^{(III)}{}_2O_4$), a ferrimagnetic mineral that saturates at low applied magnetic fields (<3 kOe) [28]. However, magnetite characteristic peaks did not appear in the XRD pattern, as its fraction was below the XRD detection limit. Heat-treated Fe nepheline shows lower magnetization and a wider hysteresis loop due to a high coercivity. This is likely due to magnetic characteristics of canted antiferromagnetic hematite ($Fe^{(III)}{}_2O_3$), which is, according to the XRD results, the dominant crystalline phase in this sample [29]. Due to the highly-disordered nature of glasses, those with magnetic elements (such as the NFS glasses) are normally paramagnetic and would not exhibit hysteresis.

No heat treatment of NBS endmember glasses yielded crystallization of a borosilicate phase. In the case of $NaBSiO_4$ for example, the glass did not nucleate after cooling at 0.5 K min^{-1} from 1200°C to 600°C followed by a 20 hr dwell. The crystalline endmember malinkoite ($NaBSiO_4$) is comprised of complex network of sheets with two types of 6-membered alternating [$SiO_{4/2}$] and [$BO_{4/2}$] ring structures [30]. To further the complexity, adjacent sheets must then fulfill a *trans* configuration. The presence of such a complex crystalline polymorph suggest that a large hindrance to crystallization lies in the restrictions in configurational entropy that must be overcome to achieve nucleation.

Additional authors have sought to understand the relationship between network structure and crystallization behavior. Lee and Stebbins [31] studied the effect of cation field strength on ordering of glasses by ^{17}O triple-quantum magic angle spinning nuclear magnetic resonance (3QMAS NMR) of $LiAlSiO_4$ and $NaAlSiO_4$ glasses. A lower degree of alumina avoidance in the LAS glass was found, suggesting greater ordering than the NAS glass. Another study sought to ascertain why lithium diborate (Li_2O-$2B_2O_3$, LB2) glass crystallizes homogeneously and sodium (Na_2O-$2B_2O_3$, NB2) glass crystallizes heterogeneously, rotational-echo double resonance (REDOR) was performed [32]. Analysis of network former/network modifier REDOR found large similarities among the amorphous and crystalline LB2 polymorphs which were not present in the NB2 polymorphs [32]. A similar conclusion was achieved when comparing the fraction of

4-coordinated boron in these systems where the LB2 polymorphs feature the same fraction of B(IV) whereas the fraction of B(IV) is significantly higher in NB2 glass than NB2 crystal [32].

CONCLUSIONS

The aim of this work was to analyze the similarities among the average structures of quenched and heat treated feldspathoid-like, pyroxene-like, and feldspar-like glasses. The glasses of $LiAlSiO_4$, $NaAlSiO_4$, and $NaFeSi_2O_6$ crystallized a stoichiometric phase upon heat treatment. Raman spectroscopy revealed an apparent broadening of the average ring structures in LAS, NAS, and NBS glasses as a function of increasing Si fraction. Hysteresis curves of the NFS glasses revealed a tendency to form iron oxide species after heat treatment below the detection limit of XRD. Although more rigorous modelling is required, the XPDF data demonstrated an increase in tridymite-like ring structures in all compositional systems as a function of Si addition.

ACKNOWLEDGEMENTS

This work was supported by funding provided by the Federal Project Director, William F. Hamel, Jr, of the Department of Energy (DOE), Waste Treatment & Immobilization Plant (WTP), under the direction of Dr. Albert Kruger, contract number DE-EM002904. The authors would like to thank Dr. Ashutosh Goel from Rutgers University for sample preparation and insight as well as Dr. Yi Gu and Xin Tao for granting access to their Raman Spectrometer.

REFERENCES

1 A.A. Kruger, Advances in Glass formulations for Hanford High-Alumina, High-Iron and Enhanced Sulphate Management in HLW streams – 13000, Department of Energy, Office of River Protection, Richland, WA, ORP-54302-FP (2013).

2 B.J. Riley, P. Hrma, J. Rosario and J.D. Vienna, In *Ceramic Transactions Vol. 132, Environmental Issues and Waste Management Technologies in the Ceramic and Nuclear Industries VII*, edited by G. L. Smith, S. K. Sundaram and D. R. Spearing, (The American Ceramic Society, Westerville, OH, 2001), pp. 257.

3 C.M. Jantzen and D.E. Bickford in *Scientific basis for Nuclear Waste Management VIII,* edited by C. M. Jantzen, J. A. Stone and R. C. Ewing, (Mater. Res. Soc. Symp. Proc. **44**, Pittsburgh, PA, 1985), pp. 135.

4 J. Marcial, J. Crum, O. Neill and J. McCloy, Amer. Mineral. **101**, 266 (2016).

5 J. Marcial, J. McCloy and O. Neill in *Scientific Basis for Nuclear Wate Management XXXVIII,* edited by S. Gin, R. Jubin, J. Matyas and E. Vance, (Proc. Mater. Res. Soc. Symp. **1744**, Boston, MA, 2015), pp. 85.

6 J. McCloy, N. Washton, P. Gassman, J. Marcial, J. Weaver and R. Kukkadapu, J. Non-cryst. Solids **409**, 149 (2015).

7 J.S. McCloy, C. Rodriguez, C. Windisch, C. Leslie, M.J. Schweiger, B.R. Riley and J.D. Vienna, In *Ceramic Transactions, Vol 222, Advances in Materials Science for Environmental and Nuclear Technology*, edited by K. M. Fox, E. N. Hoffman, N. Manjooran and G. Pickrell, (John Wiley & Sons, Inc., Hoboken, NJ, 2010), pp. 63.

8 P.B. Rose, D.I. Woodward, M.I. Ojovan, N.C. Hyatt and W.E. Lee, J. Non-cryst. Solids **357**, 2989 (2011).
9 W.A. Deer, R.A. Howie, W.S. Wise and J. Zussman, Editors,*Framework Silicates: Silica Minerals, Feldspathoids and the Zeolites*, 2nd ed. (The Geological Society, London, 2004).
10 In *An Introduction to Rock-Forming Minerals*, edited by W. A. Deer, R. A. Howie and J. Zussman, (Addison-Wesley Longman, London, 1992), pp. 473.
11 J. Marcial, J. Kabel, M. Saleh, Y. Shaharyar, A. Goel and J. McCloy, Proc. Waste Manag. Conf. 16323 (2016).
12 X. Qiu, J.W. Thompson and S.J.L. Billinge, J. Appl. Cryst. **37**, 1 (2004).
13 M. Wojdyr, J. Appl. Cryst. **43**, 3 (2010).
14 J.G. Thompson, R.L. Withers, A. Melnitchenko and S.R. Palethorpe, Acta Cryst. B **54**, 531 (1998).
15 R.L. Withers, J.G. Thompson, A. Melnitchenko and S.R. Palethorpe, Acta Cryst. B **54**, 547 (1998).
16 H.G.F. Winkler, Golden Book of Phase Transitions, Wroclaw **1**, 122 (2002).
17 D. Levy, R. Guistetto and H. Andreas, Phys. Chem. Miner. **39**, 8 (2012).
18 P. Schouwink, L. Dubrovinsky, K. Glazyrin, M. Merlini, M. Hanfland, T. Pippinger and R. Miletich, Am. Mineral. **96**, 6 (2011).
19 M.J. Buerger, G.E. Klein and G.E. Hamburger, Bull. Geol. Soc. Amer. **57**, 2 (1946).
20 K. Momma and F. Izumi, J. Appl. Crystallogr. **44**, 4 (2011).
21 M. Taylor and G.E. Brown Jr, Geochim. Cosmochim. Acta **43**, 1467 (1979).
22 C.M.S. Dan Sykes, J. Geophys. Res. **951**, 4 (1990).
23 D.W. Matson, S.K. Sharma and J.A. Philpotts, Amer. Mineral. **71**, 694 (1986).
24 E.M. Pierce, L.R. Reed, W.J. Shaw, B.P. McGrail, J.P. Icenhower, C.F. Windisch, E.A. Cordova and J. Broady, Geochim. Cosmochim. Act. **74**, 2634 (2010).
25 K. Onuma, T. Iwai and Y. Kenzo, J. Fac. Sci., Hokk. U. Ser. 4, Geol. Mineral. **15**, 179 (1972).
26 J.C.P. de Oliveira, M.I. da Costa Jr., W.H. Schreiner, A. Vasquez, N. Vieira Jr. and A. Roisenberg, J. Magn. Magn. Mater. **75**, 5 (1988).
27 O. Ballet, J.M.D. Coey, G. Fillion, A. Ghose, A. Hewat and J.R. Regnard, Phys. Chem. Miner. **16**, 6 (1989).
28 R.M. Cornell and U. Schwertmann, *The Iron Oxides: Structure, Properties, Reactions, Occurrences and Uses, 2nd, Completely Revised and Extended Edition*, 2, (John Wiley & Sons, Hoboken, 2003).
29 M. Ahmadzadeh, A. Ataie and E. Mostafavi, J. Alloys Compd. **622**, 9 (2015).
30 E.V. Sokolova, F.C. Hawthorne and A.P. Khomyakov, Can. Mineral. **39**, 159 (2001).
31 S.K. Lee and J.F. Stebbins, J. Non-cryst. Solids **270**, 260 (2000).
32 E.D. Zanotto, J.E. Tsuchida, J.F. Schneider and H. Eckert, Int. Mater. Rev. **60**, 16 (2015).